11th International Symposium on Turbulence and Shear Flow Phenomena (TSFP11)
Southampton, UK, July 30 to August 2, 2019

INSTANTANEOUS STRUCTURES OF 3D TURBULENT VELOCITY FIELDS RECONSTRUCTED WITH 4DVAR

Yi Li
School of Mathematics and Statistics
University of Sheffield
Sheffield, S3 7RH
yili@sheffield.ac.uk

ABSTRACT

4D Variational data assimilation has been used in numerical weather prediction for some time. The technique has been adopted by the fluid dynamic community recently, and has been applied in, e.g., inflow condition generation for large eddy simulations, velocity fields reconstruction from measurement data, and sensor placement (see, e. g., Gronskis *et al.* (2013); Foures *et al.* (2014); Mons *et al.* (2016, 2017)). These studies, however, are mostly limited to 2D or steady flows. The technique has not been fully examined in 3D turbulence where multi-scale interactions and the instantaneous vortical structures dominate. In this paper, we investigate the reconstruction of 3D fully developed turbulent velocity fields using the 4D variational (4DVar) method. To assess the reconstruction of non-local structures, minimum volume enclosing ellipsoids (MVEEs) are introduced. The comparisons between the MVEEs for the instantaneous non-local structures show that 4DVAR can reproduce the locations, orientations and sizes of non-local structures with good accuracy towards the end of the optimization horizon. The relative displacement of the centers of the MVEEs is about 20% of the length of the major axis. The reconstructed structures tend to be somewhat smaller, with the most probable ratio of the major axes being 80%. The alignment between the structures, on the other hand, is excellent, with more than 90% MVEES aligned within 26° in the major axis direction.

INTRODUCTION

Four dimensional variational (4DVAR) data assimilation uses available experimental or observational data to improve computational model predictions, by solving a constrained optimization problem. Spatial as well as temporal data are assimilated into the model by minimizing the difference between the model prediction and the data. In recent years, 4DVAR has been applied to fluid dynamic problems (Hayase, 2015). Gronskis *et al.* (2013) applies the variational method to reconstruct the inflow and initial conditions for two-dimensional (2D) mixing layers and wake flows behind a cylinder. Mons *et al.* (2016) considers 2D wake flows, where a comprehensive comparison between different DA schemes is presented. RANS models are investigated with variational methods in (Foures *et al.*, 2014). In D'adamo *et al.* (2007), Artana *et al.* (2012), and Protas *et al.* (2015), variational methods are coupled with reduced order models based on Galerkin truncation. Variational methods are also used in state estimation in the context of flow control (Bewley & Protas, 2004; Chevalier *et al.*, 2006; Colburn *et al.*, 2011), to extrapolate experimental data in a dynamically consistent way (Heitz *et al.*, 2010; Combes *et al.*, 2015) and to obtain optimal sensor placements (Mons *et al.*, 2017). A list of recent works on DA is tabulated in Mons *et al.* (2017)). However, few studies have examined the ability of 4DVAR to reconstruct instantaneous structures in 3D turbulent fields. In this paper, we consider a homogeneous fully developed Kolmogorov flow in a 3D periodic box. It is assumed that a time sequence of velocity data are given on a set of grid points. 4DVAR is employed to reconstruct the initial velocity field such that the velocity at later times matches given measurement data. The time sequence of velocity fields computed from the initial field are compared with the 'true' velocity fields. The objective is to ascertain how well the instantaneous small scale velocity fields can be reconstructed.

To evaluate the reconstruction of small scale *non-local structures*, it is important to quantify the geometry of the structures. The morphology of non-local structures have long been described with visualization. Great efforts have been made in recent years to develop methods for quantitative description, using curvatures, curvelets and angular spectra, among others (Bermejo-Moreno & Pullin, 2008; Yang & Pullin, 2011; Leung *et al.*, 2012). These methods provide very detailed quantitative descriptions of the structures. However, they focus on the intrinsic geometry; the information about locations, orientations and sizes of the structures sometimes is missing, which is important when we compare the geometry in two different fields. We propose to use minimum volume enclosing ellipsoids (MVEEs) to describe the geometry of a nonlocal structure, and use MVEE trees where the structures are highly non-convex. MVEE is used widely in areas such as statistical estimate, cluster analysis and image processing (Todds, 2016). Our results demonstrate that MVEEs and MVEE trees are useful tool for the analysis of the non-local geometry in turbulence.

PROBLEM SETUP

We assume the velocity on a set of spatial locations $\mathbf{x} \in \Omega$ from a time sequence of 3D unsteady velocity fields $\mathbf{v}(\mathbf{x},t)$ ($\mathbf{x} \in B$) are known over a time period $t \in [0,T]$, where B is the 3D periodic box. The known velocity, denoted as $\mathscr{F}\mathbf{v}(\mathbf{x},t)$, serves as the 'measurement data'. $\mathscr{F}$ is a filter

that extracts the velocity for $\mathbf{x} \in \Omega$. Let $\mathbf{u}(\mathbf{x},t)$ be a solution of the Navier-Stokes equations (NSEs) with initial condition $\mathbf{u}(\mathbf{x},0) = \boldsymbol{\phi}(\mathbf{x})$. The goal is to reconstruct the initial velocity field $\boldsymbol{\phi}(\mathbf{x})$ and $\mathbf{u}(\mathbf{x},t)$ for $t \leq T$, such that $\mathbf{u}(\mathbf{x},t)$ agrees with $\mathbf{v}(\mathbf{x},t)$ for $\mathbf{x} \in \Omega$. The reconstruction is conducted using the four-dimensional variational method, where we define a cost functional to quantify the difference between $\mathbf{u}(\mathbf{x},t)$ and the measurement data:

$$J \equiv \frac{1}{2}\int_0^T \int_B ||\mathscr{F}(\mathbf{u}(\mathbf{x},t) - \mathbf{v}(\mathbf{x},t))||^2 d^3\mathbf{x}dt, \qquad (1)$$

where T is the optimization horizon. The initial field $\boldsymbol{\phi}(\mathbf{x})$ is found from a constrained optimization problem in which J is minimized subject to the constraint that $\mathbf{u}(\mathbf{x},t)$ is the solution of the NS equation given $\boldsymbol{\phi}(\mathbf{x})$ as the initial condition. Using the adjoint method, the optimal solution is found by solving the optimality system:

$$\mathbf{N}(\mathbf{u}) \equiv -\partial_t \mathbf{u} - \mathbf{u}\cdot\nabla\mathbf{u} - \nabla p + \nu\nabla^2\mathbf{u} + \mathbf{f} = 0, \qquad (2)$$

with $\nabla\cdot\mathbf{u} = 0$, $\mathbf{u}(\mathbf{x},0) = \boldsymbol{\varphi}(\mathbf{x})$, and

$$-\partial_t\boldsymbol{\xi} - \mathbf{u}\cdot\nabla\boldsymbol{\xi} + \nabla\mathbf{u}\cdot\boldsymbol{\xi} + \nabla\sigma - \nu\nabla^2\boldsymbol{\xi} - \mathbf{F} = 0, \qquad (3)$$

with $\nabla\cdot\boldsymbol{\xi} = 0$, $\boldsymbol{\xi}(\mathbf{x},T) = 0$. The forcing term $\mathbf{F}$ in Eq. (3) is

$$\mathbf{F}(\mathbf{x},t) \equiv -\frac{\partial J}{\partial \mathbf{u}} = -\mathscr{F}^+\mathscr{F}[\mathbf{u}(\mathbf{x},t) - \mathbf{v}(\mathbf{x},t)] \qquad (4)$$

where $\mathscr{F}^+$ is the adjoint operator of $\mathscr{F}$. The optimality system is closed by $DJ/D\boldsymbol{\varphi} = 0$ where $DJ/D\boldsymbol{\varphi}$ is the gradient of J with respect to $\boldsymbol{\varphi}$, given by

$$\frac{DJ}{D\boldsymbol{\varphi}} = \frac{\partial L}{\partial \boldsymbol{\varphi}} = \boldsymbol{\xi}(\mathbf{x},0). \qquad (5)$$

The optimality system is solved iteratively with the nonlinear conjugate gradient method until J is less than a small tolerance.

RESULTS AND DISCUSSIONS

For a given set of measurement data, an ensemble with 11 realizations of $\boldsymbol{\phi}(\mathbf{x})$ and corresponding $\mathbf{u}(\mathbf{x},t)$ ($t \in [0,T]$) are computed for $T = 0.4\tau_L$ and 2 realizations for $T = 0.5\tau_L$. Each realization consists of a time sequence of velocity fields. In all cases, 128^3 grid points are used. The statistics of $\boldsymbol{\phi}$ and $\mathbf{u}(\mathbf{x},t)$ are calculated from the ensemble. For the cases considered in this paper, the measurement data $\mathscr{F}\mathbf{v}(\mathbf{x},t)$ contain only the large scale components of $\mathbf{v}(\mathbf{x},t)$, given by the first a few Fourier modes of the latter. $\mathbf{v}$ is obtained from a direct numerical simulation (DNS). Therefore, $\mathbf{u}(\mathbf{x},t)$ (including $\mathbf{u}(\mathbf{x},0) \equiv \boldsymbol{\phi}(\mathbf{x})$) can be viewed as a reconstruction of $\mathbf{v}(\mathbf{x},t)$ based on partial data $\mathscr{F}\mathbf{v}$. $\mathbf{u}(\mathbf{x},t)$ is compared to $\mathbf{v}(\mathbf{x},t)$ to ascertain to what extent the reconstruction captures the small scale instantaneous structures in $\mathbf{v}$. As a reference, the energy spectrum $E(k)$ of $\boldsymbol{\phi}(\mathbf{x})$ is shown in Fig. 1, which shows that the energy spectrum of

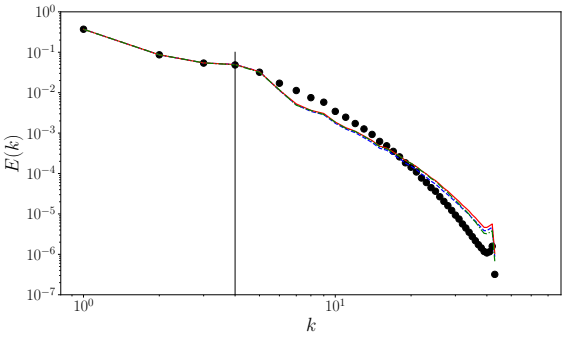

Figure 1. The energy spectrum $E(k)$ of $\boldsymbol{\phi}$ (lines) compared with DNS data (solid circles). The measurement data contain the Fourier modes with wavenumber up to the value marked by the vertical line.

$\boldsymbol{\phi}$ is reconstructed satisfactorily, although some discrepancy is observed at small scales.

To illustrate the reconstruction of instantaneous structures, Fig. 2 compares the contours of an instantaneous target vorticity field to its reconstruction. The two figures display high level of similarity. In particular, the peak values are close to each other, and are observed at about the same locations. Therefore, Fig. 2 demonstrates qualitatively the ability of 4DVar to reconstruct instantaneous structures. To quantitatively assess the similarity between the contours (or the isosurfaces in 3D), MVEEs are used following the following procedure.

In step one, the set $\mathscr{P}$ of the grid points where certain threshold condition is satisfied are extracted. $\mathscr{P}$ usually consists of a number of disjoint regions. Each disjoint region is defined as a nonlocal structure.

In step two, individual structures in $\mathscr{P}$ are isolated from others. It is accomplished by using a clustering algorithm called DBSCAN (Ester *et al.*, 1996; Schubert *et al.*, 2017). The algorithm is based on the definition of 'neighbors'. A neighbor of point p is a point whose distance to p is less than a given small value ε_c. A point with fewer than n_c neighbors is 'noise'. A cluster is defined by the following rule: the neighbors of a non-noise point p are in the same cluster as point p. Starting from point p, the 'neighbors' of p in $\mathscr{P}$ are first identified, the above rule is then applied recursively until all the points identified are noise. This identifies the cluster containing p. The same process is then repeated for other non-noise points. For more details of the DBSCAN algorithm, the readers are referred to Ester *et al.* (1996).

In step three, the MVEE for each structure is calculated. Note that, mathematically, an ellipsoid is defined by a symmetric positive definite matrix E and a vector $\mathbf{c}$. The eigenvectors and eigenvalues of E specifies the orientations and lengths of the axes of the ellipsoid. $\mathbf{c}$ specifies its center. The volume of the ellipsoid is proportional to the determinant of $E^{1/2}$, $\det E^{1/2}$. Let P be the set of points p_i ($i = 1,...,N$) in a structure. The MVEE of the structures is then given by the optimal E and $\mathbf{c}$ that minimize $\det E^{1/2}$, subject to the constraints

$$(p_i^T - \mathbf{c}^T)E^{-1}(p_i - \mathbf{c}) \leq 1, \quad \forall p_i \in P. \qquad (6)$$

The constraints make sure that p_i is inside the ellipsoid, so that the ellipsoid encloses the structure. This mini-

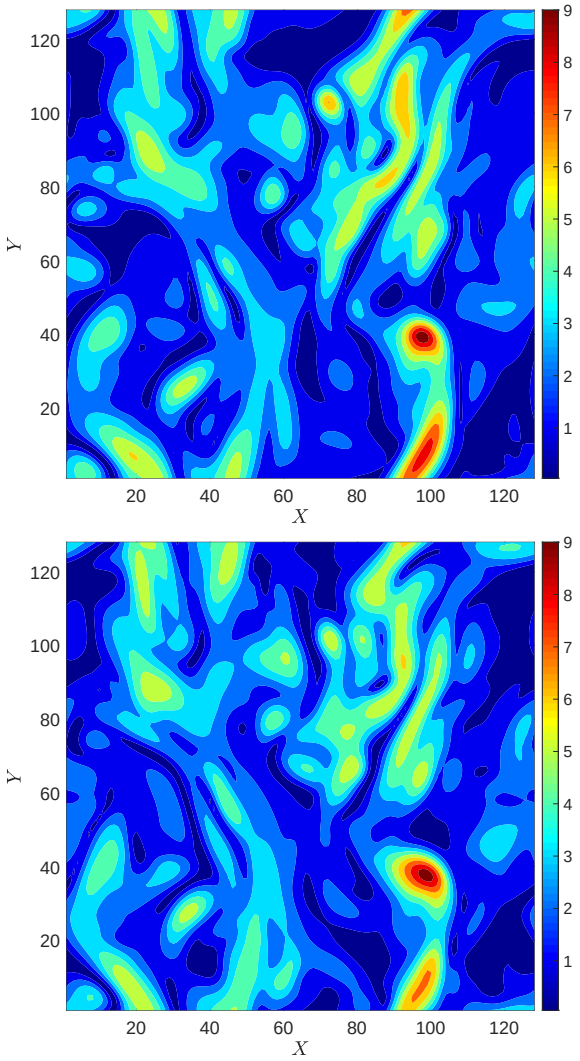

Figure 2. Instantaneous distributions of $\tilde{\omega} \equiv (\tilde{\omega}_i \tilde{\omega}_i)^{1/2}$ on a plane perpendicular to the z axis. Left: from a target field; right: from the corresponding reconstructed field.

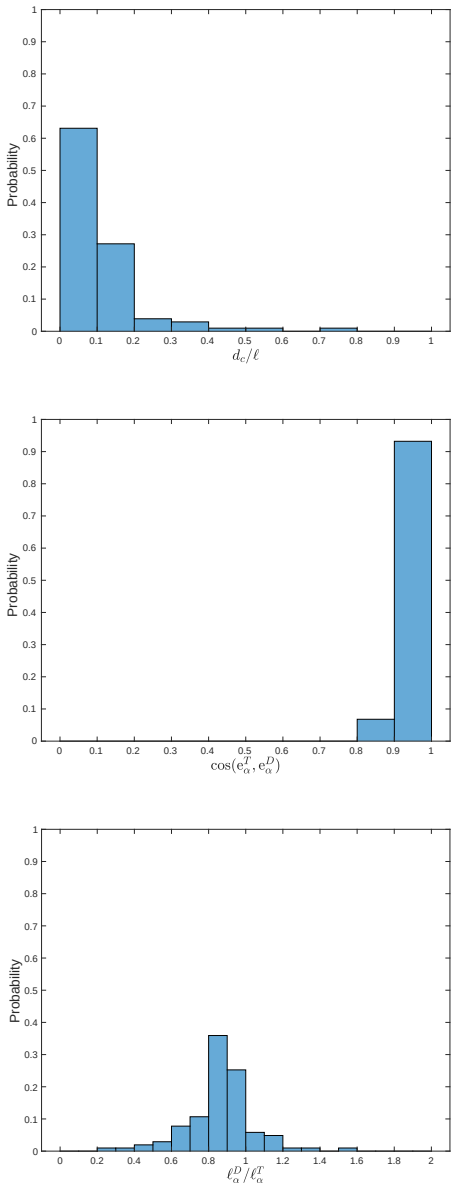

Figure 3. Top: the probability distribution of the distance between the centers of the MVEEs in the major axis direction normalized by the length of the major axis of the MVEE in $\mathbf{v}(\mathbf{x},t)$ for $t = T$ with $T = 0.4\tau_L$. Middle: the probability distribution of the cosine between the major axes of the MVEEs. Bottom: the probability distribution of the ratio of the lengths of the major axes of the MVEEs.

mization problem is solved with the Khachiyan algorithm (Khachiyan, 1996; Todds, 2016).

The fourth (and last) step establishes the correspondence between a structure in the target field and its reconstruction in the reconstructed field. The above three steps are applied to both the reconstructed and the target fields, yielding two groups of MVEEs. The following procedure is then used to identify the corresponding structures. The structures in the target field are first ordered into a list in the descending order of their sizes, where the *size* of a structure is defined as the number of grid points in the structure. Let $\mathscr{S}_T$ be a structure in the list. The structure $\mathscr{S}_O$ in the reconstructed field whose distance to $\mathscr{S}_T$ is the minimum is then identified. If $\mathscr{S}_O$ is not unique, the one largest in size is chosen as $\mathscr{S}_O$. $\mathscr{S}_O$ is taken as the reconstruction of $\mathscr{S}_T$. $\mathscr{S}_T$ and $\mathscr{S}_O$ are called the *matching* structures.

The matching structures and corresponding MVEEs obtained this way are then compared in terms of the relative displacement, alignment, and relative sizes, among others. The instantaneous vortical structures in $\mathbf{u}(\mathbf{x},t)$ and $\mathbf{v}(\mathbf{x},t)$ are compared this way, and the results are shown in Fig. 3. The vortical structures are defined as domains where $|\boldsymbol{\omega}|$ is three times larger than its mean value (the flow fields are first filtered with a Gaussian filter with length scale $\Delta \approx 10\eta_K$). The top panel of Fig. 3 shows the probability distribution of the relative displacement between the centers of the MVEEs found in $\mathbf{u}(\mathbf{x},t)$ and $\mathbf{v}(\mathbf{x},t)$, normalized by the length of the axis. That is, $d_c = |(\mathbf{c}^T - \mathbf{c}^D) \cdot \mathbf{e}_\alpha^T|$ and ℓ is the length the major axis of the MVEE in the target field, where superscripts T and D represent the target field and the reconstructed field, respectively, and $\mathbf{e}_\alpha$ represents the major axis direction. The result (calculated at $t = T$ for $T = 0.4\tau_L$) shows that, in more than 60% cases, the displacement of the two MVEEs is less than 10% of the length of the axis, and in more than 85% cases, the displacement is less than 20%. The middle panel of Fig. 3 plots the probability distribution of the cosine of the major axes of

the two MVEEs found in $\mathbf{u}(\mathbf{x},t)$ and $\mathbf{v}(\mathbf{x},t)$. Perfect alignment occurs when the cosine is unit. The figure shows that the orientations of the two structures align nearly perfectly, with the cosine is larger than 0.9 (with the angle smaller than 26°) in more than 90% cases. Finally, the bottom panel plots the probability distribution of the ratio of the lengths of the major axes. The result shows that the reconstructed MVEEs tend to somewhat smaller than the target MVEEs. The most probable ratio is 80%. About 60% ratios are between 80$\sim$ 100%, which demonstrates high probability of good agreement too.

CONCLUSIONS

The 4DVar method has been used to reconstruct instantaneous non-local structures in 3D turbulent fields from incomplete velocity data. Minimum volume enclosing ellipsoids (MVEEs) are used to characterize the irregular shapes of the structures. Results on the alignment, relative displacement of the MVEEs, and the ratio of the axis lengths show that the vortical structures in the reconstructed fields agree well with those in the true fields. More detailed comparison will be presented in the future, including the time evolution of the structures, the reconstruction of the non-local structures in the subgrid-scale energy dissipation field and the strain rate field.

REFERENCES

Artana, G., Cammilleri, A., Carlier, J. & Memin, E. 2012 Strong and weak constraint variational assimilations for reduced order fluid flow modeling. *Journal of Computational Physics* **231**, 3264–3288.

Bermejo-Moreno, I. & Pullin, D. I. 2008 On the non-local geometry of turbulence. *Journal of Fluid Mechanics* **603**, 101–135.

Bewley, T. R. & Protas, B. 2004 Skin friction and pressure: the "footprints" of turbulence. *Physica D* **196**, 28–44.

Chevalier, M., Hoepffner, J., Bewley, T. R. & Henningson, D. S. 2006 State estimation in wall-bounded flow systems. part 2. turbulent flows. *Journal of Fluid Mechanics* **552**, 167–187.

Colburn, C. H., Cessna, J. B. & Bewley, T. R. 2011 State estimation in wall-bounded flow systems. part 3. the ensemble kalman filter. *Journal of Fluid Mechanics* **682**, 289–303.

Combes, B., Heitz, D., Guibert, A. & Memin, E. 2015 A particle filter to reconstruct a free-surface flow from a depth camera. *Fluid Dyn. Res.* **47**, 051404.

D'adamo, J., Papadakis, N., Memin, E. & Artana, G. 2007 Variational assimilation of pod low-order dynamical systems. *Journal of Turbulence* **8**, N9.

Ester, M., Kriegel, H.-P., Sander, J. & Xu, X. 1996 A density-based algorithm for discovering clusters in large spatial databases with noise. *KDD-96 Proceedings* **1**, 226–231.

Foures, D. P. G., Dovetta, N., Sipp, D. & Schmid, P. J. 2014 A data-assimilation method for reynolds-averaged navier-stokes-driven mean flow reconstruction. *J. Fluid Mech.* **759**.

Gronskis, A., Heitz, D. & Memin, E. 2013 Inflow and initial conditions for direct numerical simulation based on adjoint data assimilation. *J. Comput. Phys.* **242**, 480–497.

Hayase, T. 2015 Numerical simulation of real-world flows. *Fluid Dynamics Research* **47**, 051201.

Heitz, D., Memin, E. & Schnorr, C. 2010 Variational fluid flow measurements from image sequences: synopsis and perspectives. *Exp. Fluids* **48**, 369–393.

Khachiyan, L. G. 1996 Rounding of polytopes in the real number model of computation. *Mathematics of Operations Research* **21**, 307–320.

Leung, T., Swaminathan, N. & Davidson, P. A. 2012 Geometry and interaction of structures in homogeneous isotropic turbulence. *Journal of Fluid Mechanics* **710**, 453–481.

Mons, V., Chassaing, J.-C., Gomez, T. & Sagaut, P. 2016 Reconstruction of unsteady viscous flows using data assimilation schemes. *Journal of Computational Physics* **316**, 255–280.

Mons, V., Chassaing, J.-C. & Sagaut, P. 2017 Optimal sensor placement for variational data assimilation of unsteady flows past a rotationally oscillating cylinder. *J. Fluid Mech.* **823**, 230–277.

Protas, B., Noack, B. R. & Osth, J. 2015 Optimal nonlinear eddy viscosity in galerkin models of turbulent flows. *Journal of Fluid Mechanics* **766**, 337–367.

Schubert, Erich, Sander, Jörg, Ester, Martin, Kriegel, Hans Peter & Xu, Xiaowei 2017 Dbscan revisited, revisited: Why and how you should (still) use dbscan. *ACM Trans. Database Syst.* **42** (3), 19:1–19:21.

Todds, M. J. 2016 *Minimum-Volume Ellipsoids: Theory and Algorithms*. SIAM.

Yang, Y. & Pullin, D. I. 2011 Geometric study of eulerian and lagrangian structures in turbulent channel flows. *Journal of Fluid Mechanics* **674**, 67–92.